
This is an electronic reprint of the original article.
This reprint may differ from the original in pagination and typographic detail.

Hinkkanen, Marko; Harnefors, Lennart; Luomi, Jorma

Control of induction motor drives equipped with small DC-link capacitance

Published in:

12th European Conference on Power Electronics and Applications (EPE2007)

DOI:

[10.1109/EPE.2007.4417763](https://doi.org/10.1109/EPE.2007.4417763)

Published: 02/09/2007

Document Version

Peer-reviewed accepted author manuscript, also known as Final accepted manuscript or Post-print

Please cite the original version:

Hinkkanen, M., Harnefors, L., & Luomi, J. (2007). Control of induction motor drives equipped with small DC-link capacitance. In *12th European Conference on Power Electronics and Applications (EPE2007)* (European Conference on Power Electronics and Applications). <https://doi.org/10.1109/EPE.2007.4417763>

This material is protected by copyright and other intellectual property rights, and duplication or sale of all or part of any of the repository collections is not permitted, except that material may be duplicated by you for your research use or educational purposes in electronic or print form. You must obtain permission for any other use. Electronic or print copies may not be offered, whether for sale or otherwise to anyone who is not an authorised user.

Control of Induction Motor Drives Equipped With Small DC-Link Capacitance

Marko Hinkkanen
HELSINKI UNIVERSITY
OF TECHNOLOGY
P.O. BOX 3000
FI-02015 TKK, Finland
marko.hinkkanen@tkk.fi

Lennart Harnefors
ABB POWER SYSTEMS
PS/G/DC/TST
SE-77180 Ludvika, Sweden
lennart.harnefors@se.abb.com

Jorma Luomi
HELSINKI UNIVERSITY
OF TECHNOLOGY
P.O. BOX 3000
FI-02015 TKK, Finland
jorma.luomi@tkk.fi

Keywords

«Control of drive», «Converter control», «Induction motor»

Abstract

The paper deals with control of induction motor drives equipped with a diode rectifier and a small dc-link capacitance. Neither an ac choke nor a dc choke is used. It is necessary to use dc-link stabilization control if the mains inductance is not very low. Conventional dc-link stabilization controllers rely on the current controller. If no input choke is used, however, the natural frequency of the dc link is higher than the current-control bandwidth, and the conventional stabilization methods cannot be used. This paper proposes a control algorithm based on direct manipulation of the stator voltage reference. Furthermore, a recently proposed field-weakening controller is modified to better suit the oscillating dc-link voltage. Design recommendations for the proposed scheme are presented. Simulation results of a 110-kW drive show that the proposed scheme stabilizes the dc link and the dynamic performance is comparable with that of the conventional drive.

1 Introduction

Frequency converters used in induction motor drives are usually equipped with a six-pulse diode rectifier, a voltage-stiff dc link, and a pulse-width-modulated inverter. Conventionally, the dc link is based on electrolytic capacitors and a dc choke (or an ac choke at the input of the rectifier), and the natural frequency of the dc link is much lower than six times the mains frequency. There is an increasing interest in replacing the electrolytic capacitors by film capacitors having a longer lifetime and no explosion risks, but the dc-link capacitance has to be considerably reduced in order not to increase the size of the capacitor bank.

Small dc-link capacitances have been applied in ac drives equipped with active rectifiers [1], where both the rectifier and the inverter can be used to control the power balance of the dc link. Commercial drives equipped with a diode rectifier and a small dc-link capacitance are available [2]; a small capacitance is advertised to reduce the mains harmonics, while the dynamic performance of the drive has not been used as an argument. In research publications, the concept of a diode rectifier and a small dc-link capacitance has received little attention, with the exception of recent studies: pulse-width modulation (PWM) was studied in [3, 4], and control issues relating to 2.2-kW and 37-kW drives were studied in [5].

Instability of the dc link may occur in conventional drives (having a low dc-link natural frequency), if the inductance of a choke is large relative to the dc-link capacitance. The dc link can be stabilized by manipulating the reference of the torque-producing current component [6, 7, 8]. If a small dc-link capacitance without an additional choke is used, the dc-link natural frequency becomes high and dependent on the mains inductance. Especially in large-power drives, the mains inductance relative to the dc-link capacitance may be large enough to cause instability in the dc link, while the dc-link natural frequency is above the bandwidth of the current-control loop. Hence, conventional stabilization methods relying on the current controller cannot be used.

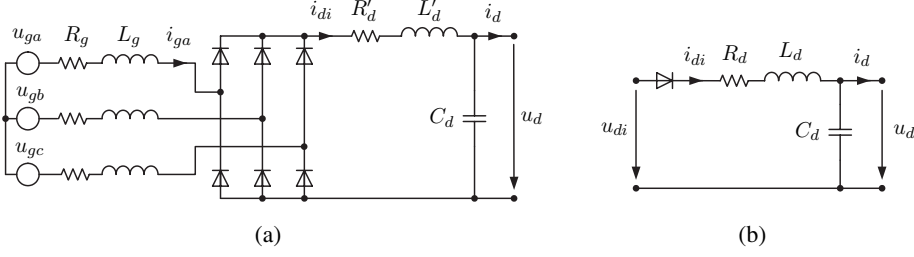


Fig. 1: Mains, diode rectifier, and dc link: (a) typical model; (b) simplified model.

In this paper, control of sensorless rotor-flux oriented drives equipped with a small dc-link capacitance without an additional choke is studied. In an example drive of 110-kW rated power, the dc-link capacitance is a tenth of the conventional one, and natural frequencies are in the range of 300...1500 Hz depending on the mains inductance. The natural frequencies are lower than those in [5] but several times higher than those in [6, 7, 8]. A method for stabilizing the dc link directly by modifying the stator voltage reference is proposed. Furthermore, the field-weakening controller of [9] is modified to better suit the oscillating dc-link voltage. The proposed scheme is analyzed by means of linearization and simulations.

2 System Model

2.1 Diode Rectifier and DC Link

The models of the drive system components are presented in the following. Fig. 1(a) shows a three-phase model of the mains, the diode rectifier, and the dc link. The mains resistance and inductance¹ are denoted by R_g and L_g , respectively, and the dc-link inductance, resistance, and capacitance are L'_d , R'_d , and C_d , respectively. The phase-to-neutral mains voltages u_{ga} , u_{gb} , and u_{gc} for a balanced three-phase system have the peak value u_g and the angular frequency ω_g . The current at the output of the rectifier is i_{di} , while the current and voltage at the input of the inverter are i_d and u_d , respectively. The inverter is not shown in the figure. It is modeled by three ideal changeover switches.

The model in Fig. 1(a) is approximated by a simplified model in Fig. 1(b). The ideal rectified voltage is $u_{di} = \max\{u_{ga}, u_{gb}, u_{gc}\} - \min\{u_{ga}, u_{gb}, u_{gc}\}$, or in terms of its harmonic components

$$u_{di} = u_{di,av} \left[1 - \sum_{n=1}^{\infty} \frac{2}{(6n)^2 - 1} \cos(6n\omega_g t) \right] \quad (1)$$

where the average is $u_{di,av} = 3\sqrt{3}u_g/\pi$. The parameters are $L_d = L'_d + 2L_g$ and $R_d = R'_d + 2R_g + 3\omega_g L_g/\pi$, where the term $3\omega_g L_g/\pi$ corresponds to the non-ohmic voltage drop due to commutation [10]. The differential equations

$$L_d \frac{di_{di}}{dt} = u_{di} - u_d - R_d i_{di}, \quad C_d \frac{du_d}{dt} = i_{di} - i_d, \quad i_{di} \geq 0 \quad (2)$$

correspond to Fig. 1(b).

2.2 Induction Motor and Mechanics

The dynamic model corresponding to the inverse- Γ equivalent circuit [11] of the induction motor will be used. The electrical dynamics in general coordinates rotating at arbitrary angular speed ω_k are given by

$$L_\sigma \frac{d\mathbf{i}_s}{dt} + \omega_k L_\sigma \mathbf{J} \mathbf{i}_s = \mathbf{u}_s - R_\sigma \mathbf{i}_s + (\alpha \mathbf{I} - \omega_m \mathbf{J}) \boldsymbol{\psi}_R, \quad \frac{d\boldsymbol{\psi}_R}{dt} + \omega_k \mathbf{J} \boldsymbol{\psi}_R = R_R \mathbf{i}_s - (\alpha \mathbf{I} - \omega_m \mathbf{J}) \boldsymbol{\psi}_R \quad (3)$$

where $\mathbf{J} = \begin{bmatrix} 0 & -1 \\ 1 & 0 \end{bmatrix}$ is the orthogonal rotation matrix, $\mathbf{u}_s = [u_{sd}, u_{sq}]^T$ the stator voltage vector, $\mathbf{i}_s = [i_{sd}, i_{sq}]^T$ is the stator current, $\boldsymbol{\psi}_R = [\psi_{Rd}, \psi_{Rq}]^T$ is the rotor flux, and ω_m is the electrical angular speed

¹If an ac choke is used, its resistance and inductance should be included in R_g and L_g , respectively.

of the rotor. The stator resistance is R_s , the rotor resistance is R_R , the total resistance is $R_\sigma = R_s + R_R$, the magnetizing inductance is L_M , the total leakage inductance is L_σ , and the inverse rotor time constant is $\alpha = R_R/L_M$.

Peak-value scaling of vectors is used. Hence, the electromagnetic torque is $T_e = (3/2)p\mathbf{i}_s^T \mathbf{J}\psi_R$, where p is the number of pole pairs. The equation of motion is given by $(J/p)d\omega_m/dt = T_e - T_L - b\omega_m/p$, where J is the total moment of inertia of the mechanical system, T_L the load torque, and b the viscous friction coefficient. The losses in the inverter will be neglected for simplicity. Hence, the power p_s into the stator equals the the power into the inverter:

$$p_s = \frac{3}{2}\mathbf{i}_s^T \mathbf{u}_s = u_d i_d \quad (4)$$

3 Stabilization of DC Link

3.1 Linearized Model of DC Link and Stability Condition

The system (2) has two inputs: the ideal rectified voltage u_{di} and the current i_d at the inverter input. Since $i_d = p_s/u_d$ according to (4), the dynamics of the dc link are nonlinear. The stability of the dc link can be analyzed using a small-signal linearized model. The system behavior on time scales longer than the switching period is described by averaging the variables over one switching period. The deviation of the current i_d can be expressed as $\tilde{i}_d = (\partial i_d/\partial p_s)_0 \tilde{p}_s + (\partial i_d/\partial u_d)_0 \tilde{u}_d = \tilde{u}_d/R_0 + \tilde{p}_s/u_{d0}$, where \tilde{i}_d , \tilde{u}_d , and \tilde{p}_s refer to deviations about the operating point, and the operating-point quantities are marked by the subscript 0. The parameter $R_0 = -u_{d0}^2/p_{s0}$ depends on the operating point and is negative in the motoring mode. Hence, the linearized small-signal model becomes

$$L_d \frac{d\tilde{i}_{di}}{dt} = \tilde{u}_{di} - \tilde{u}_d - R_d \tilde{i}_{di}, \quad C_d \frac{d\tilde{u}_d}{dt} = \tilde{i}_{di} - \tilde{u}_d/R_0 - \tilde{p}_s/u_{d0} \quad (5)$$

where the current i_{di} at the output of the rectifier is assumed to be continuous. From (5), the transfer function from the power $\tilde{p}_s(s)$ to the dc-link voltage $\tilde{u}_d(s)$ becomes

$$\frac{\tilde{u}_d(s)}{\tilde{p}_s(s)} = -\frac{1}{u_{d0}} \frac{sL_d + R_d}{s^2 L_d C_d + s(R_d C_d + L_d/R_0) + 1 + R_d/R_0} \quad (6)$$

The poles of (6) are located at $-\zeta\omega_n \pm j\omega_n\sqrt{1-\zeta^2}$, where the parameters

$$\omega_n = \sqrt{\frac{R_0 + R_d}{R_0} \frac{1}{L_d C_d}} \approx \sqrt{\frac{1}{L_d C_d}}, \quad \zeta = \frac{1}{2\omega_n} \left(\frac{R_d}{L_d} + \frac{1}{R_0 C_d} \right) \quad (7)$$

are the undamped natural frequency and the damping ratio of the system, respectively. Since the damping ratio ζ should be positive, the stability condition [8]

$$C_d/p_{s0} > L_d/(R_d u_{d0}^2) \quad (8)$$

is obtained. If no dc choke is used, i.e. $L_d = 2L_g$, and the losses in the dc link and in the mains are insignificant, i.e. $R_d = 3\omega_g L_g/\pi$, the ratio $L_d/R_d = 2\pi/(3\omega_g)$. In this case, the condition equals $C_d/p_{s0} > 23 \mu\text{F/kW}$ if the dc-link voltage is $u_{d0} = 540$ V and the mains angular frequency $\omega_g = 2\pi 50$ rad/s.

Since the duty cycles are calculated based on the measured dc-link voltage, the motor dynamics (or the power \tilde{p}_s) are ideally independent of the dc-link dynamics. If the PWM saturates, however, the stator voltage \tilde{u}_s depends on the dc-link voltage \tilde{u}_d . Hence, the dynamics of the dc link in (5) couple with those of the motor and controllers, and the stability condition (8) may not hold. The saturation of the PWM can be prevented by controlling the motor flux level so that there is always some voltage margin.

3.2 Control Law

If the dc-link capacitance is small, the stability condition (8) may not be fulfilled. In this case, the dc link can be stabilized by controlling the deviation \tilde{p}_s of the power. Here, ideal control of the inverter output power is assumed. Hence, a proportional controller can be considered,

$$\tilde{p}_s(s) = k_{ud} p_{s0} \tilde{u}_d(s) / u_{d0} \quad (9)$$

where the controller gain k_{ud} is a nonnegative constant. The damping ratio of the closed-loop system formed by (6) and (9) is $\zeta_{cl} = [R_d/L_d + (1 - k_{ud})/(R_0 C_d)] / (2\omega_{n,cl})$, where $\omega_{n,cl} \approx \omega_n$. The second term in the brackets can be made to vanish by choosing $k_{ud} = 1$. Using this selection, the damping of the dc link equals the damping in no-load operation.

If the bandwidth of current control is significantly higher than the natural frequency ω_n of the dc link, the inverter output power \tilde{p}_s can be controlled by manipulating the stator current reference [6, 8]. In the case of a small dc-link capacitance and no input choke, however, the natural frequency ω_n is usually higher than the bandwidth of current control. Hence, the power \tilde{p}_s cannot be controlled via the current reference, but the stator voltage reference has to be manipulated directly.

Based on (3), the operating-point stator voltage is $\mathbf{u}_{s0} = \mathbf{Z}_0 \mathbf{i}_{s0}$, where the impedance is

$$\mathbf{Z}_0 = R_s \mathbf{I} + \omega_{s0} \mathbf{J} [L_\sigma \mathbf{I} + R_R (\alpha \mathbf{I} + \omega_{r0} \mathbf{J})^{-1}] \quad (10)$$

where $\omega_{r0} = \omega_{s0} - \omega_{m0}$ is the slip angular frequency. In synchronous coordinates rotating at ω_{s0} , the relationship between the voltage and current deviations is $\tilde{\mathbf{u}}_s(s) = \mathbf{Z}(s) \tilde{\mathbf{i}}_s(s)$, where the impedance is

$$\mathbf{Z}(s) = R_\sigma \mathbf{I} + (s \mathbf{I} + \omega_{s0} \mathbf{J}) L_\sigma - R_R (\alpha \mathbf{I} - \omega_{m0} \mathbf{J}) (s \mathbf{I} + \alpha \mathbf{I} + \omega_{r0} \mathbf{J})^{-1} \quad (11)$$

Hence, the deviation of the power can be expressed as

$$\tilde{p}_s(s) = \frac{3}{2} [\mathbf{i}_{s0}^T \tilde{\mathbf{u}}_s(s) + \mathbf{u}_{s0}^T \tilde{\mathbf{i}}_s(s)] = \frac{3}{2} \mathbf{i}_{s0}^T \mathbf{G}(s) \tilde{\mathbf{u}}_s(s) \quad (12)$$

where $\mathbf{G}(s) = \mathbf{I} + \mathbf{Z}_0^T \mathbf{Z}^{-1}(s) = G_d(s) \mathbf{I} + G_q(s) \mathbf{J}$ is a dimensionless transfer-function matrix. At higher frequencies, the impedance (11) can be approximated as $\mathbf{Z}(s) \approx R_\sigma \mathbf{I} + (s \mathbf{I} + \omega_{s0} \mathbf{J}) L_\sigma$, yielding

$$G_d(s) = 1 + \frac{(s L_\sigma + R_\sigma) \left(R_s + \frac{\omega_{r0} \omega_{s0}}{\alpha^2 + \omega_{r0}^2} R_R \right) - \omega_{s0} L_\sigma \left(\omega_{s0} L_\sigma + \frac{\alpha \omega_{s0}}{\alpha^2 + \omega_{r0}^2} R_R \right)}{(s L_\sigma + R_\sigma)^2 + \omega_{s0}^2 L_\sigma^2} \quad (13)$$

$$G_q(s) = - \frac{(s L_\sigma + R_\sigma) \left(\omega_{s0} L_\sigma + \frac{\alpha \omega_{s0}}{\alpha^2 + \omega_{r0}^2} R_R \right) + \omega_{s0} L_\sigma \left(R_s + \frac{\omega_{r0} \omega_{s0}}{\alpha^2 + \omega_{r0}^2} R_R \right)}{(s L_\sigma + R_\sigma)^2 + \omega_{s0}^2 L_\sigma^2} \quad (14)$$

Different control strategies could be developed for the system (12). A simple algorithm is obtained by fixing the coordinates to the operating-point stator current, i.e. $\mathbf{i}_{s0} = [i_{s0}, 0]^T$, and exploiting only the d component of the stator voltage. Hence, the multiple-input-single-output system (12) reduces to a single-input-single-output system $\tilde{p}_s(s) = (3/2) i_{s0} G_d(s) \tilde{u}_{sd}(s)$, and the control law (9) can be expressed as

$$\tilde{u}_{sd}(s) = \frac{2}{3 i_{s0}} G_d^{-1}(s) \tilde{p}_s(s) = k_{ud} \frac{u_{sd0}}{u_{d0}} G_d^{-1}(s) \tilde{u}_d(s) \quad (15)$$

Since only higher frequencies are of interest, the transfer function $G_d^{-1}(s)$ can be approximated

$$G_d^{-1}(s) \approx \frac{s + 2R_\sigma/L_\sigma}{s + \left(2R_\sigma + R_s + \frac{\omega_{r0} \omega_{s0}}{\alpha^2 + \omega_{r0}^2} R_R \right) / L_\sigma} \quad (16)$$

With this approximation, the controller (15) can be interpreted as a gain-scheduled lead-lag compensator. Fig. 2(a) illustrates the frequency response of $G_d^{-1}(s)$ obtained from the original expression and from the high-frequency approximation (16). It can be seen that the accuracy of the approximation (16) is sufficient since the frequencies above 300 Hz are of interest.

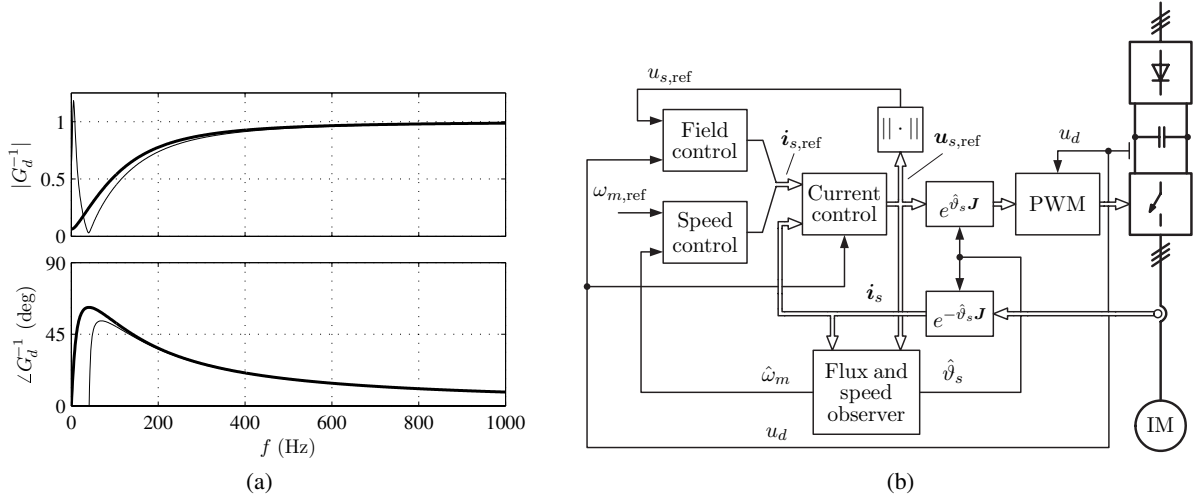


Fig. 2: (a) Original frequency response of $G_d^{-1}(s)$ (thin line) and approximation (16) (thick line). Parameters of a 110-kW motor were used, and $\omega_{s0} = 0.8$ p.u. and $\omega_{r0} = 0.013$ p.u. (b) Simplified block diagram of rotor-flux-oriented control system. Block “Current control” includes current controller and dc-link stabilization controller. Block “Field control” includes field weakening controller.

3.3 Implementation

In the estimated rotor flux coordinates, the stator voltage reference including the dc-link stabilization signal is

$$\mathbf{u}_{s,\text{ref}} = e^{\vartheta_i \mathbf{J}} \begin{bmatrix} 1 + K(s)u_d & 0 \\ 0 & 1 \end{bmatrix} e^{-\vartheta_i \mathbf{J}} \mathbf{u}_{s,\text{ref}0} \quad (17)$$

where $\mathbf{u}_{s,\text{ref}0}$ is the reference obtained from the current controller, ϑ_i is the angle of the stator current vector, and $K(s)$ is the stabilizing control law (here, s should be interpreted as the operator $s = d/dt$). To avoid noise in the angle ϑ_i , it can be calculated as $\vartheta_i = \arctan(\hat{\omega}_r/\alpha)$, where the estimated slip angular frequency $\hat{\omega}_r = R_R \hat{i}_{sq} / \hat{\psi}_R$ and $\hat{\psi}_R$ is obtained from the flux observer. The deviation $\tilde{u}_d = u_d - u_{d0}$ of the dc-link voltage can be obtained by high-pass filtering, $\tilde{u}_d = s/(s + \alpha_1)u_d$, where the bandwidth α_1 should be low to avoid phase errors in \tilde{u}_d (much lower than the natural frequency of the dc link). Based on (15) and (16), the selection $\alpha_1 = 2R_\sigma/L_\sigma$ results in a stabilizing controller

$$K(s) = \frac{k_{ud}}{u_{d0}} \frac{s}{s + \alpha_2}, \quad \alpha_2 = \left(2R_\sigma + R_s + \frac{\hat{\omega}_r \omega_s}{\alpha^2 + \hat{\omega}_r^2} R_R \right) / L_\sigma \quad (18)$$

where α_2 depends on the operating point and u_{d0} can be replaced with the nominal value of the dc-link voltage. It is worth noticing that PWM should be able to realize the stabilization signal superimposed on the stator voltage reference. Hence, the switching frequency should be sufficiently higher than the dc-link natural frequency.

4 Field-Weakening Control

4.1 Control Law

The small dc-link capacitance does not ideally cause loss of the maximum fundamental stator voltage. However, the overmodulation may cause low-frequency oscillations at $|6(\omega_g - \omega_s)|$ in the stator voltage magnitude u_s if the dc-link capacitance is small [3]. These oscillations are caused by the interaction of two phenomena: (i) the oscillation of the dc-link voltage u_d at the frequency of $6\omega_g$ appears in the stator voltage when overmodulating; and (ii) the overmodulation itself causes the harmonics at $6\omega_s$ in the stator voltage (even if the dc-link voltage u_d is constant). To avoid the oscillations, the voltage reference $\mathbf{u}_{s,\text{ref}}$ is limited to the linear modulation range, i.e., $u_{s,\text{ref}} = \|\mathbf{u}_{s,\text{ref}}\| \leq u_d/\sqrt{3}$ even in transients.

Conventionally, field weakening is achieved by decreasing the flux reference inversely proportionally to the rotor speed. To guarantee the control of the stator current, a large voltage margin is usually provided, leading to a reduction in the maximum torque. Furthermore, the actual voltage margin depends on the operating point. Since the voltage margin is worth minimizing in practice, the flux reference can be determined based on the error between the reference voltage and the maximum steady-state voltage [12].

A simpler method—a modified version of [9]—is obtained by excluding the conventional flux controller; the flux-producing current reference is controlled and limited according to

$$\frac{di_{sd,\text{ref}}}{dt} = \lambda (u_{s,\text{max}} - u_{s,\text{ref}}), \quad -i_{s,\text{max}} \leq i_{sd,\text{ref}} \leq i_{sdN} \quad (19)$$

where λ is the controller gain, $u_{s,\text{max}}$ is the maximum stator voltage in steady state, and i_{sdN} is the rated value of the flux-producing current component. The maximum steady-state voltage is calculated based on the dc-link voltage according to $u_{s,\text{max}} = k_{us}u_d/\sqrt{3}$, where the positive constant $k_{us} \leq 1$ determines the voltage margin. In the case of the conventionally dimensioned dc link, $k_{us} = 1$ can be selected if the overmodulation region is used, while $k_{us} < 1$ is needed in the case of the small dc-link capacitance. Since the overmodulation cannot be used for the voltage margin, the maximum steady-state voltage is lower when the dc-link capacitance is small than in the case of the conventionally dimensioned dc-link capacitance.

4.2 Gain Selection

Ideal current control and ideal PWM are considered in the following, i.e., $\mathbf{i}_s = \mathbf{i}_{s,\text{ref}}$ and $\mathbf{u}_s = \mathbf{u}_{s,\text{ref}}$. The linearized algorithm (19) is thus $d\tilde{i}_{sd}/dt = \lambda_0(\tilde{u}_{s,\text{max}} - \tilde{u}_s)$, where $\tilde{i}_{sd} = \boldsymbol{\psi}_{R0}^T \tilde{\mathbf{i}}_s$, $\tilde{u}_{s,\text{max}} = k_{us}\tilde{u}_d/\sqrt{3}$, and $\tilde{u}_s = \mathbf{u}_{s0}^T \tilde{\mathbf{u}}_s/u_{s0}$. The gain λ_0 determines the closed-loop rotor-flux dynamics. When these slower dynamics are considered, the stator-current dynamics in (11) can be omitted due to different time scales, leading to the approximate impedance²

$$\mathbf{Z}(s) \approx R_\sigma \mathbf{I} + \omega_{s0} L_\sigma \mathbf{J} - R_R (\alpha \mathbf{I} - \omega_{m0} \mathbf{J}) (s \mathbf{I} + \alpha \mathbf{I} + \omega_{r0} \mathbf{J})^{-1} \quad (20)$$

The transfer function from $\tilde{i}_{sd}(s)$ to $\tilde{u}_s(s)$ is $Z(s) = \mathbf{u}_{s0}^T \mathbf{Z}(s) \boldsymbol{\psi}_{R0} / (u_{s0} \psi_{R0})$, where the operating-point stator voltage is $\mathbf{u}_{s0} = R_s \mathbf{i}_{s0} + \omega_{s0} \mathbf{J} (L_\sigma \mathbf{i}_{s0} + \boldsymbol{\psi}_{R0}) \approx \omega_{s0} \mathbf{J} \boldsymbol{\psi}_{R0}$. The transfer function corresponding to the control algorithm (19) is $L(s) = \lambda_0/s$. The closed-loop rotor-flux dynamics are

$$\frac{\tilde{u}_s(s)}{\tilde{u}_{s,\text{max}}(s)} = \frac{L(s)Z(s)}{1 + L(s)Z(s)} \quad (21)$$

The gain $\lambda_0 = 2R_R/(L_\sigma^2|\omega_{s0}|)$ yields the poles of (21) approximately at $(-1 \pm j)R_R/L_\sigma$, whereas a smaller λ_0 reduces the damping. Based on the pole locations, the closed-loop rotor-flux dynamics (21) are sufficiently fast. The gain can be implemented as $\lambda = 2R_R\hat{\psi}_R/(L_\sigma^2\psi_{RN})$, where ψ_{RN} is the rated rotor flux. The dc-link dynamics couple with the dynamics of the motor and controllers through $\tilde{u}_{s,\text{max}}$ when operating in the field-weakening region. However, the coupling is weak since the current controller bandwidth is lower than the dc-link natural frequency. Furthermore, using the limited voltage reference in (19) reduces the effect of oscillating \tilde{u}_d on the flux dynamics.

5 Control System

A simplified block diagram of the speed-sensorless rotor-flux-oriented control system is shown in Fig. 2(b). The proposed dc-link stabilizing controller and field-weakening controller are used. If an electronically controlled braking resistor across the dc link is not used, the field-weakening controller could be augmented with the braking scheme presented in [13]. A PI current controller operating in estimated rotor flux coordinates is used, the current controller bandwidth being 4 p.u. The bandwidth of

²The system (20) can be expressed as a state-space representation: $d\tilde{\boldsymbol{\psi}}_R/dt = -(\alpha \mathbf{I} + \omega_{r0} \mathbf{J}) \tilde{\boldsymbol{\psi}}_R + R_R \tilde{\mathbf{i}}_s$; $\tilde{\mathbf{u}}_s = -(\alpha \mathbf{I} - \omega_{m0} \mathbf{J}) \tilde{\boldsymbol{\psi}}_R + (R_\sigma \mathbf{I} + \omega_{s0} L_\sigma \mathbf{J}) \tilde{\mathbf{i}}_s$, where $\tilde{\mathbf{i}}_s$ is the input and $\tilde{\mathbf{u}}_s$ is the output.

the PI speed controller—including the active damping [9]—is 0.08 p.u. The maximum stator current is $i_{s,\max} = 1.5$ p.u.

Conventional space-vector PWM and synchronized sampling (once per carrier half-period) are used in the simulations; the switching frequency is 4 kHz, and the sampling frequency is 8 kHz. The duty cycles are determined in the beginning of the carrier half-period using the dc-link voltage u_d measured in the beginning of the previous carrier half-period. The sampling delay and the change of u_d during the carrier period cause some errors in the produced stator voltage \mathbf{u}_s . The accuracy of the stator voltage could be improved by measuring u_d several times per carrier half-period and by determining the switching instants on line during the carrier half-period [4].

The rotor flux estimate (whose amplitude is denoted by $\hat{\psi}_R$ and angle by $\hat{\vartheta}_s$) and the rotor speed estimate $\hat{\omega}_m$ are obtained using a speed-adaptive flux observer [14]. The measured stator current \mathbf{i}_s and the stator voltage reference $\mathbf{u}_{s,\text{ref}}$ are the inputs of the flux observer. PWM cannot perfectly compensate the effects of the oscillating dc-link voltage on the voltage \mathbf{u}_s , leading to noise in the stator current. Furthermore, a current controller migrates noise at lower frequencies to the voltage reference $\mathbf{u}_{s,\text{ref}}$. Consequently, when a small dc-link capacitance is used, the damping of the flux observer is more important than usually due to the increased noise content.

6 Simulation Results

The speed-sensorless induction motor drive described in the previous section was investigated by means of simulations. The rated values of the 110-kW induction motor used in the simulations are: speed 1481 r/min; frequency 50 Hz; line-to-line rms voltage 380 V; rms current 200 A; and torque 708 Nm. Motor parameters are: $R_s = 0.012$ p.u.; $R_R = 0.012$ p.u.; $L_\sigma = 0.231$ p.u.; $L_M = 3.640$ p.u. The total moment of inertia is $J = 200$ p.u. (two times the inertia of the rotor alone) and the viscous friction coefficient $b = 0$. The mains frequency is 50 Hz and the line-to-line rms voltage 400 V. Two mains inductances of 20 μH and 120 μH will be considered. The mains inductance of 20 μH approximately equals the short-circuit inductance of a 2-MVA 20-kV/400-V 50-Hz distribution transformer while 120 μH corresponds to the mains inductance in [5], where the drive was fed by a 500-kVA 20-kV/400-V 50-Hz distribution transformer. The dc-link inductance $L'_d = 0$ is assumed. The mains resistance $R_g = 0$ and the dc-link resistance $R'_d = 0$ are assumed corresponding to the worst-case damping, resulting in the resistance $R_d = 3\omega_g L_g / \pi$. In the conventional dc link, $C_d = 5.7$ mF (corresponding to $C_d/P_N = 52$ $\mu\text{F}/\text{kW}$) and an ac choke of 110 μH are used. As a small dc-link capacitance, $C_d = 0.44$ μF (corresponding to $C_d/P_N = 4$ $\mu\text{F}/\text{kW}$), while no input choke is used.

Fig. 3 shows results of an acceleration and a speed reversal. The speed reference is stepped from zero to 1 p.u. at $t = 0.1$ s. The rated load torque is applied stepwise at $t = 1$ s. The first subplot shows the rotor speed (thick line) and its reference (thin line). The second subplot shows the stator current components (thick) and their references (thin) in the estimated rotor flux coordinates. The third subplot presents the dc-link voltage u_d divided by $u_{di,\text{av}} = 540$ V. The last subplot shows the dc-link voltage u_d and the ideal rectified voltage u_{di} within the period of $t = 1.20 \dots 1.22$ s. As a reference, results of the drive equipped with the conventional dc link—having the natural frequency of 131 Hz—are depicted in Fig. 3(a). The overmodulation region is used as voltage margin, and the whole linear modulation region can be used in steady state, i.e. $k_{us} = 1$. The dc-link stabilization algorithm is disabled, i.e. $k_{ud} = 0$.

Fig. 3(b) shows simulation results of the drive equipped with the small dc-link capacitance when the mains inductance is 20 μH , yielding the dc-link natural frequency of 1.2 kHz. To prevent low-frequency oscillation, the overmodulation region is not used at all, and the voltage margin is guaranteed choosing $k_{us} = 0.96$. This selection yields the voltage margin (and dynamics) approximately equal to that of the conventional drive. However, the maximum steady-state voltage is 4 % smaller than that in the conventional drive. The dc-link stabilization controller is disabled, i.e. $k_{ud} = 0$, to demonstrate that the dc link is stable due to its high natural frequency. The selection $k_{ud} = 1$ could be used as well, leading to results

similar to Fig.3(b). The linearized model predicts that the dc link should be unstable without active stabilization. This contradiction between the simulation results and the linearized model (whose variables are averaged over a switching period) is not surprising since the dc-link natural frequency is high, and close to the switching frequency of 4 kHz.

In Fig. 3(c), the mains inductance is 120 μH and the dc-link natural frequency is 490 Hz. The dc-link stabilization controller is disabled, and the dc link is unstable when the inverter output power is high. The simulation results in Fig. 3(d) correspond to Fig. 3(c), except that the dc-link stabilization controller is enabled with $k_{ud} = 1$. The dc link is stable, and the ripple in the stator current components is decreased.

Fig. 4 depicts results where the speed reference is stepped from zero to 1.2 p.u. and a rated load torque step is applied at $t = 1$ s. The explanations of the first two subplots are as in Fig. 3. The third subplot shows the rotor flux and the last subplot depicts the dc-link voltage u_d . Results obtained using the conventional dc link are shown in Fig. 4(a) as a reference. The results in Fig. 4(b) correspond to the small capacitance and the mains inductance of 120 μH . The dc-link stabilizing controller is enabled with $k_{ud} = 1$ and the voltage margin corresponds to $k_{us} = 0.96$. The system is stable. The ripple in the current components, and in the torque increases with increasing power.

Results of an acceleration to a speed of 3 p.u. are shown in Fig. 5(a) for the drive with the conventional dc link and in Fig. 5(b) for the small dc-link capacitance. The dc-link stabilizing controller with $k_{ud} = 1$ is used in Fig. 5(b), and the voltage margin corresponds to $k_{us} = 0.96$. The acceleration time is slightly longer in Fig. 5(b) since the overmodulation region is disabled.

7 Conclusions

A small dc-link capacitance can be used without input choke if active stabilization of the dc link is used. Since the natural frequency of the dc link without the input choke is usually above the bandwidth of the current-control loop, conventional stabilization methods relying on the current controller cannot be used. The controller proposed in this paper superimposes the stabilization signal on the stator voltage reference. Furthermore, the voltage margin needed for transients can be minimized by controlling the motor flux based on the actual stator voltage and the instantaneous maximum stator voltage depending on the dc-link voltage. The simulation results of a 110-kW drive show that the proposed scheme stabilizes the dc link. The maximum steady-state voltage is slightly smaller than that of the conventional drive. The dynamic performance of the drive equipped with the small dc-link capacitance is comparable with that of the conventional drive.

References

- [1] J. S. Kim and S. K. Sul, "New control scheme for AC-DC-AC converter without DC link electrolytic capacitor," in *Proc. IEEE PESC'93*, vol. 1, Seattle, WA, June 1993, pp. 300–306.
- [2] Siemens Building Technologies Inc., "Harmonics White Paper," 2002. [Online]. Available: <http://www.sbt.siemens.com/HVP/Components/Documentation/SI033WhitePaper.pdf>
- [3] H. Sarén, O. Pyrhönen, K. Rauma, and O. Laakkonen, "Overmodulation in voltage source inverter with small dc-link capacitor," in *Proc. IEEE PESC'05*, Recife, Brazil, June 2005.
- [4] H. Sarén, O. Pyrhönen, J. Luukko, O. Laakkonen, and K. Rauma, "Verification of frequency converter with small dc-link capacitor," in *Proc. EPE'05*, Dresden, Germany, Sept. 2005.
- [5] M. Hinkkanen and J. Luomi, "Induction motor drives equipped with diode rectifier and small dc-link capacitance," in *Proc. IEEE IECON'05*, Raleigh, NC, Nov. 2005, pp. 1498–1503.
- [6] S. D. Sudhoff, K. A. Corzine, S. F. Glover, H. J. Hegner, and H. N. Robey, Jr., "DC link stabilized field oriented control of electric propulsion systems," *IEEE Trans. Energy Convers.*, vol. 13, no. 1, pp. 27–33, Mar. 1998.
- [7] H. Mosskull, "Stabilization of an induction motor drive with resonant input filter," in *Proc. EPE'05*, Dresden, Germany, Sept. 2005.

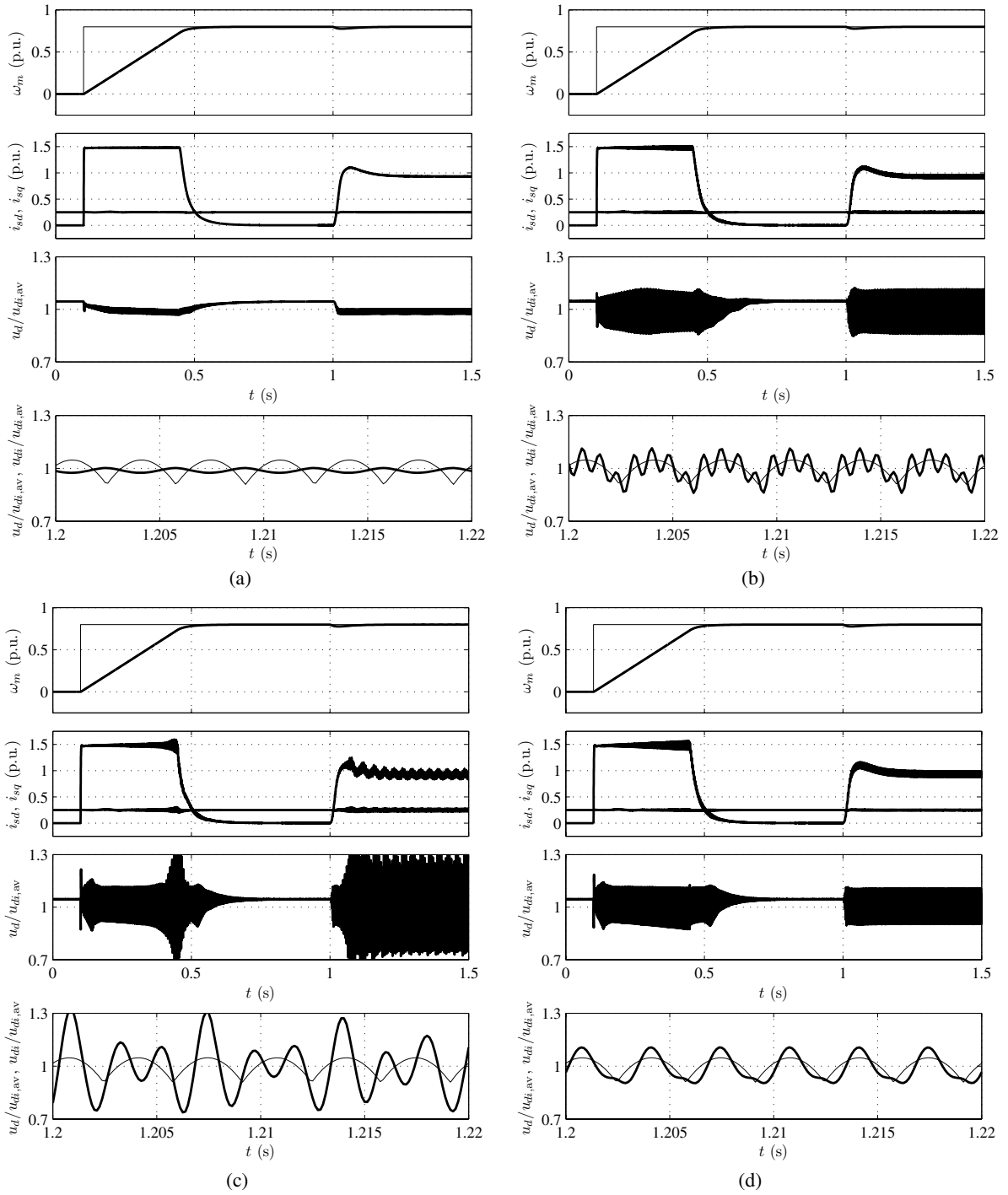


Fig. 3: Acceleration and load torque step: (a) conventional dc link, dc-link stabilization disabled; (b) small capacitance and mains inductance of $20 \mu\text{H}$, dc-link stabilization disabled; (c) small capacitance and mains inductance of $120 \mu\text{H}$, dc-link stabilization disabled; (d) small capacitance and mains inductance of $120 \mu\text{H}$, dc-link stabilization enabled.

- [8] K. Pietiläinen, L. Harnfors, A. Petersson, and H. Nee, "DC-link stabilization and voltage sag ride-through of inverter drives," *IEEE Trans. Ind. Electron.*, vol. 53, no. 4, pp. 1261–1268, Aug. 2006.
- [9] L. Harnfors, K. Pietiläinen, and L. Gertmar, "Torque-maximizing field-weakening control: design, analysis, and parameter selection," *IEEE Trans. Ind. Electron.*, vol. 48, no. 1, pp. 161–168, Feb. 2001.
- [10] P. C. Krause, O. Wasynczuk, and S. D. Sudhoff, *Analysis of Electric Machinery and Drive Systems*. Piscataway, NJ: IEEE Press, 2002.

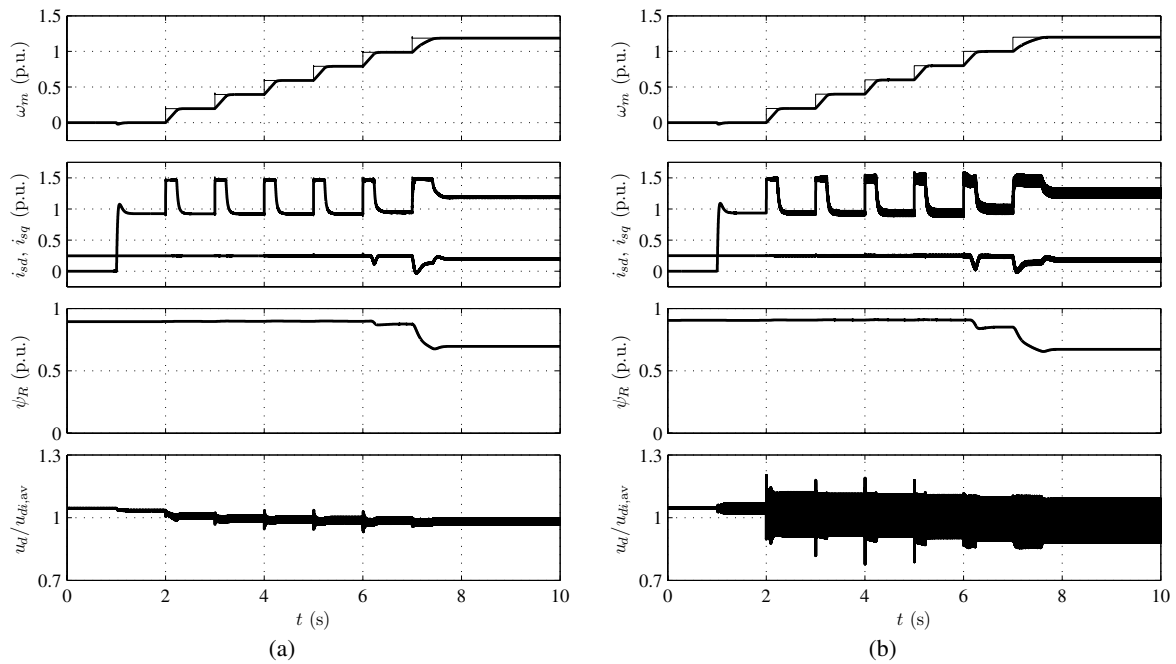


Fig. 4: Speed reference steps under rated load torque: (a) conventional dc link, dc-link stabilization disabled; (b) small capacitance and mains inductance of 120 μH , dc-link stabilization enabled.

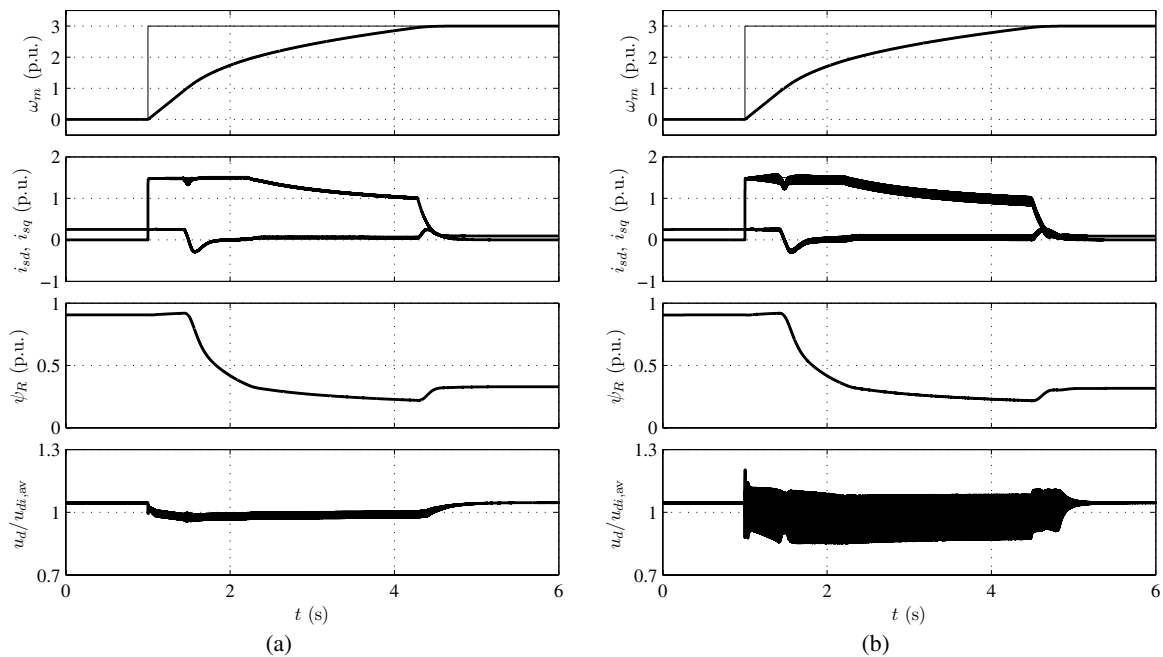


Fig. 5: High-speed operation: (a) conventional dc link, dc-link stabilization disabled; (b) small capacitance and mains inductance of 120 μH , dc-link stabilization enabled.

- [11] G. R. Slemon, "Modelling of induction machines for electric drives," *IEEE Trans. Ind. Appl.*, vol. 25, no. 6, pp. 1126–1131, Nov./Dec. 1989.
- [12] H. Grotstollen and J. Wiesing, "Torque capability and control of a saturated induction motor over a wide range of flux weakening," *IEEE Trans. Ind. Electron.*, vol. 42, no. 4, pp. 374–381, Aug. 1995.
- [13] M. Hinkkanen and J. Luomi, "Braking scheme for vector-controlled induction motor drives equipped with diode rectifier without braking resistor," *IEEE Trans. Ind. Appl.*, vol. 42, no. 5, pp. 1257–1263, Sept./Oct. 2006.
- [14] M. Hinkkanen, "Analysis and design of full-order flux observers for sensorless induction motors," *IEEE Trans. Ind. Electron.*, vol. 51, no. 5, pp. 1033–1040, Oct. 2004.